Nonalloyed Ohmic Contacts in AlGaN/GaN HEMTs With MOCVD Regrowth of InGaN for *Ka*-Band Applications

Hüseyin Çakmak, Mustafa Öztürk, Ekmel Özbay, and Bilge İmer

***Abstract*— Low-resistance ohmic contacts in AlGaN/GaN high-electron-mobility transistor (HEMT) devices require high-temperature (HT) annealing (>800 °C) which can deteriorate material quality, surface morphology, and edge acuity of the metal stacks. This article demonstrates the high-frequency and high-power performance of the AlGaN/GaN HEMT devices with low-temperature metal-organic chemical vapor deposition (MOCVD) regrown degenerately doped InGaN ohmic contacts compared with GaN-based regrown contacts. Ohmic contacts fabricated by regrowth methods could be a valuable alternative for both metal-based alloyed ohmic contacts and implantation-based ohmic contacts. Using a T-gate and MOCVD regrown InGaN ohmic contacts, the AlGaN/GaN HEMT with an L_g of 150 nm and S-D spacing of 2.5 μm demonstrated a maximum drain current of 0.94 A/mm and a peak transconductance of 337 mS/mm. The same device exhibited a forward current gain frequency f_t of 36.8 GHz and a maximum frequency of oscillation f_{max} of 75.0 GHz. A power density of 3.07 W/mm with a 60% drain efficiency was measured at 35 GHz with a V_{ds} of 20 V and a quiescent current of 100 mA/mm.**

***Index Terms*— AlGaN/GaN high-electron-mobility transistor (HEMT), metal-organic chemical vapor deposition (MOCVD), regrown InGaN ohmic contacts.**

I. Introduction

GALLIUM-NITRIDE (GaN)-based high-electron-mobility transistors (HEMTs) have had a great interest due to their unique material properties which make them promising candidates for microwave power devices compared with Si- and GaAs-based devices. Having wide bandgap (3.4 eV of GaN and 6.2 eV of AlN), high saturation electron drift velocity ($>2 \times 10^7$ cm/s), and large electrical breakdown strength ($>3 \times 10^6$ V/cm) make them suitable for harsh environment conditions [1]–[3]. Due to high electron mobility and high critical breakdown field of GaN and high thermal conductivity of SiC, these material systems demonstrate high breakdown voltages, low loss, high-speed switching, and high operating temperatures compared with Si, GaAs, and InP material systems.

Although several GaN-based devices have already reached the market, their properties are still inferior with respect to predicted performance [4]. A reliable low-resistance ohmic contacts along with smooth surface morphology and clear edge acuity are fundamental building blocks for GaN HEMT devices. A low ohmic contact resistance, R_c, is crucial for noise performance, output power, and efficiency.

To decrease the ohmic contact resistances, R_c, of GaN HEMT devices, several studies have been reported with different metallization schemes [5]–[9], implantations [7], [10], and regrown n-GaN by Molecular Beam Epitaxy (MBE) or metal-organic chemical vapor deposition (MOCVD) [11]–[13]. However, the Ti-based metal stack requires high annealing temperatures (>800 °C) which result in deteriorated surface morphology and edge acuity that affect the next coming alignment steps including gate metal lithography. Implantation also requires high activation temperatures (>1200 °C) which could affect the quality of the epitaxial layers.

In this article, we demonstrated AlGaN/GaN HEMT on the semiinsulating (SI)-SiC substrate for *Ka*-band application with the MOCVD regrown InGaN ohmic contacts. Silicon-doped InGaN ohmic contacts were grown at a surface temperature of 730 °C in the previously patterned source and drain contact regions. Plasma-Enhanced Chemical Vapor Deposition (PECVD) growth of SiO_2 was used as a mask layer for the MOCVD regrown InGaN contacts. Both dc and RF characterization was performed to investigate the performance of AlGaN/GaN HEMT devices with and without the regrown InGaN contacts.

II. Experimental Details

HEMT structures used in this article were grown on 3" SI-SiC substrates by Aixtron Epilab II MOCVD system with 3 × 3" susceptor configuration. TMAl, TMGa, Cp_2Fe, and NH_3 were used as a MO and hydride sources for epitaxial growth. The epitaxial structure along with device geometry is

Manuscript received November 19, 2020; revised December 26, 2020; accepted January 7, 2021. Date of publication January 22, 2021; date of current version February 24, 2021. This work was supported by TUBITAK-TEYDEB under Project GaNTurk 3170935. The work of Ekmel Özbay was supported in part by the Turkish Acedemy of Science. The review of this article was arranged by Editor K. J. Chen. *(Corresponding author: Bilge İmer.)*

Hüseyin Çakmak is with the AB MikroNano, 06800 Ankara, Turkey, and also with the Graduate School of Natural and Applied Science, Middle East Technical University (METU), 06800 Ankara, Turkey (e-mail: hcakmak@bilkent.edu.tr).

Mustafa Öztürk is with the AB MikroNano, Bilkent University, 06800 Ankara, Turkey (e-mail: mozturk@bilkent.edu.tr).

Ekmel Özbay is with the Nanotechnology Research Center (NANOTAM), Department of Electrical and Electronics Engineering, Institute of Materials Science and Nanotechnology (UNAM), 06800 Ankara, Turkey, and also with the Department of Physics, Bilkent University, 06800 Ankara, Turkey (e-mail: ozbay@bilkent.edu.tr).

Bilge İmer is with the Department of Metallurgical and Materials Engineering, Middle East Technical University (METU), 06800 Ankara, Turkey (e-mail: bimer@bilkent.edu.tr).

Color versions of one or more figures in this article are available at https://doi.org/10.1109/TED.2021.3050740.

Digital Object Identifier 10.1109/TED.2021.3050740

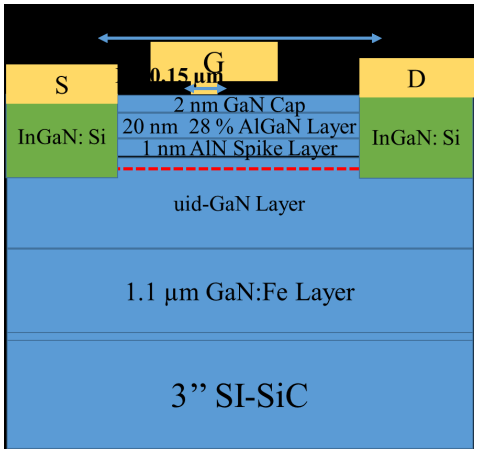

Fig. 1. Schematic representation of the fabricated AlGaN/GaN HEMT with the MOCVD regrown InGaN nonalloyed ohmic contacts.

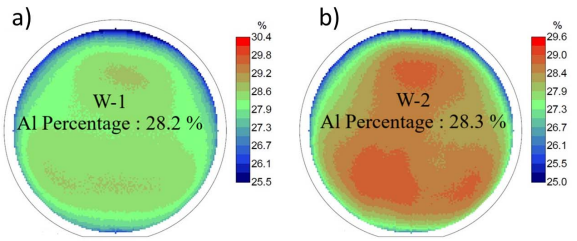

Fig. 2. PL mapping of AlGaN barrier layers of HEMT structures (a) W-1 and (b) W-2 wafers.

shown in Fig. 1. Epitaxial growth began with a 250-nm high-temperature (HT) AlN layer grown at a surface temperature of 1150 °C, followed by GaN:Fe with a thickness of 1.1 μm. A unintentional doping (UID)–GaN transition layer with a thickness of 0.8 μm was grown to avoid Fe ion diffusion to the 2-Dimentional Electron Gas (DEG) region. A channel GaN with a thickness of 200 nm was grown on the transition UID–GaN layer. The 2-DEG region was formed by growing an AlN spike layer with a thickness of around 1 and 20-nm $Al_{0.28}GaN$ barrier and capped with 2-nm GaN layer. Two SI-SiC substrates were used for epitaxial growth to make a fair performance comparison of HEMT device with and without regrown InGaN ohmic contacts. The 2-DEG properties of the HEMT structures were determined by the Lehighton Sheet Resistance mapping system where electron density, mobility, and sheet resistance measured at room temperature were around 1.2×10^{13} cm^{-3}, 1950 cm^2/V.s, and 260 Ω/sq, respectively.

The Al content of the barrier layers was determined by photoluminescence (PL) measurement system equipped with a 266-nm laser source. As seen in Fig. 2, the Al compositions of the two HEMT structures were varying around 0.1% range as an indication of good wafer-to-wafer uniformity for the MOCVD system.

Microfabrication of the HEMT with alloyed ohmic contacts (control device, W-1) started with the isolation of the active regions by etching with inductively coupled plasma reactive ion etching (ICP-RIE) using BCl_3 and Cl_2 gas chemistry. Ti, Al, Ni, and Au metals (20/100/40/50 nm) were deposited for ohmic contact formation with electron-beam evaporation followed by Rapid Thermal Annealing (RTA) annealing in

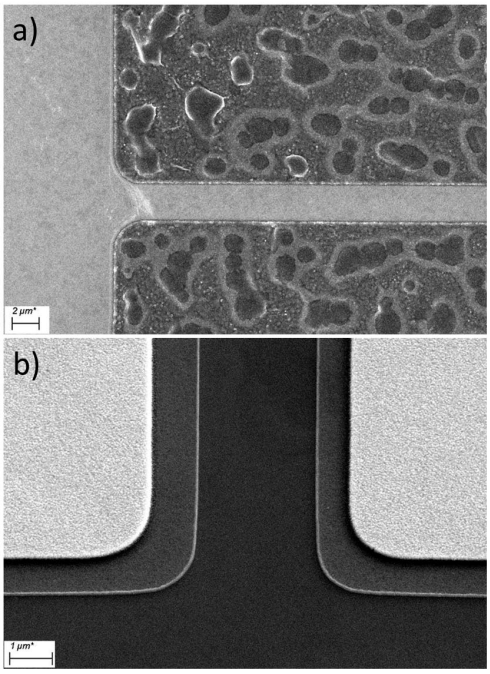

Fig. 3. Micrograph of (a) Ti-based alloyed ohmic contacts after RTA at 850 °C/45 s and (b) nonalloyed ohmic contacts.

N_2 ambient at 850 °C for 45 s. Processing of HEMT with nonalloyed ohmic contacts (W-2) started with PECVD growth of SiO_2 with a thickness of 300 nm and was patterned using standard lithography and ICP-RIE processes. Then, AlGaN/GaN heterostructure was etched down to 80 nm in the source and drain region by ICP RIE for MOCVD growth of InGaN:Si in source and contact regions. The wafer was transferred to MOCVD reactor and 90-nm $In_{0.12}GaN$:Si was grown and followed by evaporation of Cr/Au (20/100 nm) contacts. Since PECVD grown SiO_2 mask was removed by diluted HF solution right after metallization, Cr metal was chosen due to its wet etch resistance. SiO_2 masking which was used both for MOCVD growth of $In_{0.12}GaN$:Si and evaporation of Cr/Au metal stacks was lifted off by HF solution. This method also simplifies the fabrication of source and drain contacts. The rest of the HEMT fabrication was identical to have a fair comparison of the device dc and RF performance. E-beam lithography was used to define the T-shaped gate in the middle of the S–D spacing with an L_g of 0.15 μm using multiple e-beam lithography processes. A Ni/Au metal stack with a thickness of 50/450 nm was evaporated for the Schottky contact. A 75-nm PECVD Si_xN_y passivation layer was deposited. Finally, metal contact pads and air bridges were formed by the deposition of Au via electroplating processes.

The surface morphology of the Ti-based alloyed ohmic contact and nonalloyed ohmic contacts is shown in Fig. 3, below. Deteriorated surface morphology [Fig. 3(a)] and reduced edge acuity affect not only the accurate alignment of the gate electrodes for downscaled HEMTs but also the performance of the fabricated devices. The surface morphology of the MOCVD regrown InGaN nonalloyed [Fig. 3(b)] ohmic contacts exhibited much better surface morphology and edge acuity which are crucial for device fabrication and HEMT performance.

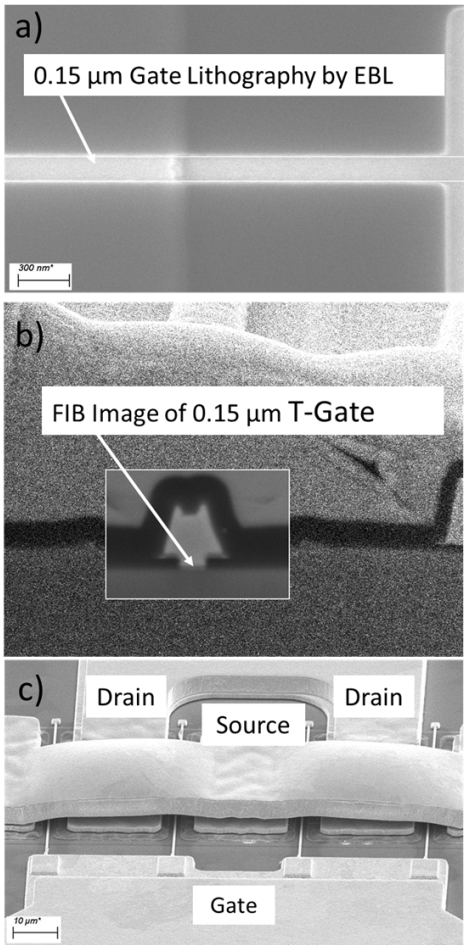

Fig. 4. Various Scanning Electron Microscope (SEM) and FIB images of HEMT device belonging to different microfabrication steps. (a) Electron beam lithography system. (b) Contact pads and air bridges. (c) FIB image of gate metal.

Fig. 4 shows the micrographs of the HEMT device after each step of the microfabrication processes including gate lithography by electron beam lithography system (a), contact pads and air bridges (b), and FIB image of gate metal (c).

III. Results and Discussions

The TLM measurements were used to analyze the ohmic contact resistivity of both the Ti-based alloyed and MOCVD regrown InGaN nonalloyed ohmic contacts. Fig. 5 shows the measurement results of the alloyed and nonalloyed ohmic contacts. As shown in Fig. 5, the total contact resistance (R_{tot}), extracted from TLM patterns, for the Ti-based alloyed and MOCVD regrown InGaN nonalloyed ohmic contacts was 0.43 Ω and 0.30 Ω·mm, respectively. Not only decreasing contact resistance but also having much better contact morphology and edge acuity compared with alloyed ohmic contacts are crucial for both device performance and device production. The lower value of R_{tot} is attributed to the degenerate doping of InGaN:Si with a carrier concentration of above 10^{20}cm^{-3} which was confirmed by Hall effect measurement of coloaded sapphire substrate during InGaN:Si growth. Barrier height lowering could be due to the pinning of the Fermi level above the conduction band of InGaN:Si. Degenerate doping of

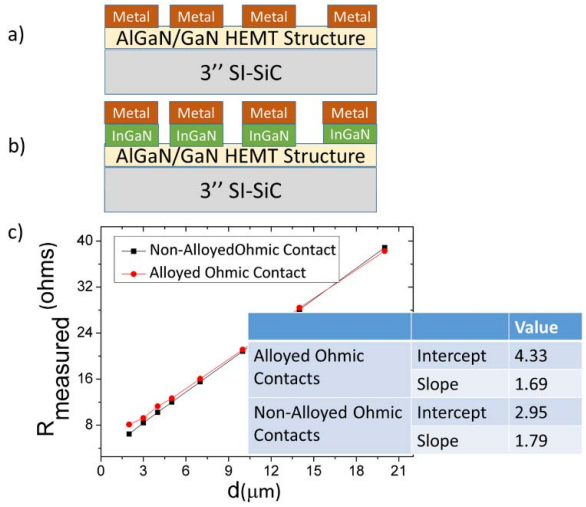

Fig. 5. TLM measurement of (a) Ti-based alloyed ohmic contacts. (b) MOCVD regrown InGaN nonalloyed ohmic contacts. (c) Resistance versus contact spacing.

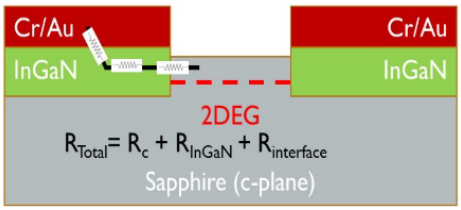

Fig. 6. Components of total contact resistances of the MOCVD regrown InGaN nonalloyed ohmic contacts.

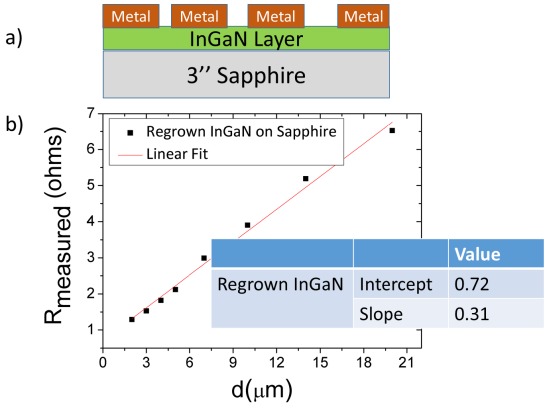

Fig. 7. Ohmic contact patterns for the MOCVD growth of InGaN on sapphire (a) and resistance versus contact spacing (b).

InGaN:Si pushes the Fermi level above the conduction band (Burstein–Moss shift) and helps form ohmic contact [14], [15].

As shown in Fig. 6, a total contact resistance R_{tot} which consists of metal/InGaN contact resistance R_c, InGaN access resistance R_{InGaN}, and InGaN/2-DEG interface $R_{\text{interface}}$ was extracted from TLM patterns.

Fig. 7 shows the TLM measurement of metal/InGaN layers. The contact resistance (R_c) was around 0.07 Ω·mm and the sheet resistance, R_{sh}, of InGaN was 62 Ω/sq. Based on the sheet resistance of InGaN layer, R_{InGaN} and $R_{\text{interface}}$ were calculated as 6×10^{-3} and 0.22 Ω·mm, respectively. The lower value of R_c than other reported values was due to the doped InGaN layers [16].

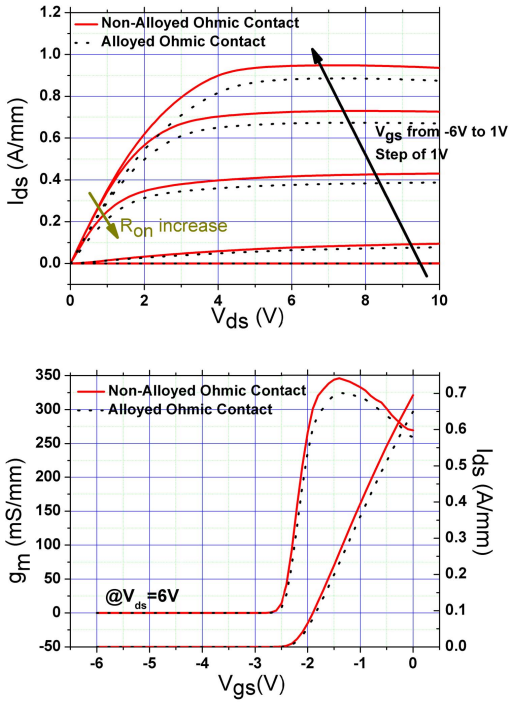

Fig. 8. Dc characteristic of alloyed and nonalloyed HEMT with $L_g = 0.15\ \mu$m ($2 \times 50\ \mu$m) and *S–D* spacing is 2.5 μm.

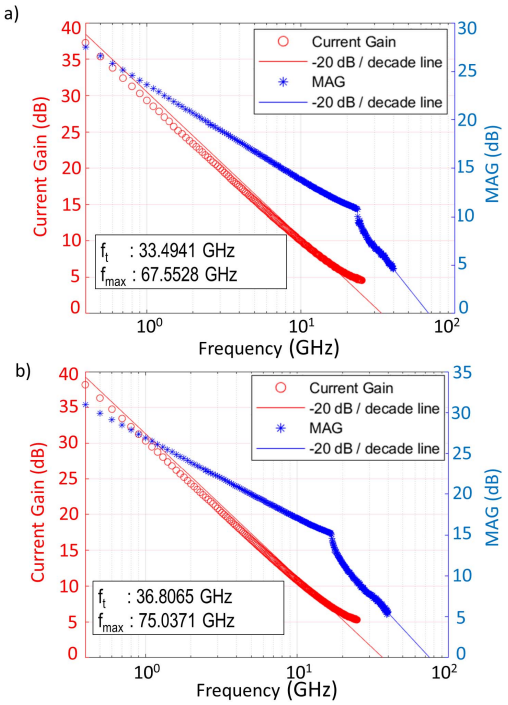

Fig. 9. Small-signal RF performance of (a) alloyed and (b) nonalloyed HEMT with $L_g = 0.15\ \mu$m and *S–D* spacing is 2.5 μm.

Lower total contact resistance, R_{tot}, and smooth surface morphology of the *S–D* contacts alleviate the technological problems of downscaled HEMT operated at higher frequencies.

The typical drain output characteristics are shown in Fig. 8. The linear region is where the drain current (I_{ds}) is proportional to the drain–source voltage (V_{ds}) and the saturation region is where I_{ds} is quasi-independent of the drain–source voltage (V_{ds}). The output characteristics of the fabricated devices with the Ti-based alloyed and MOCVD regrown InGaN nonalloyed ohmic contacts were measured.

The on resistances (R_{on}) which highly depend on the total contact resistance, R_{tot}, were extracted from the output characteristics. The measured R_{on} was 3.18 and 2.74 Ω mm for the Ti-based alloyed and MOCVD regrown InGaN nonalloyed ohmic contacts, respectively. The maximum drain current density (I_{ds}) of 0.94 and 0.88 A/mm was obtained for the sample with the MOCVD regrown InGaN nonalloyed ohmic contacts and Ti-based alloyed ohmic contacts, respectively, at $V_{\text{gs}} = 1$ V. It clearly shows that higher contact resistance for alloyed ohmic contacts has significant effects on I_{ds}. It is widely known that the RF output power of a transistor is directly proportional to the maximum available drain current density, I_{ds}. It implies that it is crucial to improve I_{ds} to increase the output power of a transistor. V_{knee} voltages, also defined as the source–drain voltage V_{ds} at which the source–drain current I_{ds} reaches 95% of its maximum value, were 3.9 and 4.2 V for the MOCVD regrown InGaN nonalloyed ohmic contacts and Ti-based alloyed ohmic contacts, respectively. The maximum transconductance, g_m, obtained for the MOCVD regrown InGaN nonalloyed ohmic contacts and Ti-based alloyed ohmic contacts was 337 and 314 mS/mm, respectively. A higher value of g_m is important to push the current gain cutoff frequency (f_t) to higher values. It is clearly seen that nonalloyed ohmic contacts have significantly improved dc characteristics of the fabricated transistors by decreasing the total contact resistance, R_{tot}. Lower access resistance and ON-resistance improved the output characteristics compared with alloyed ohmic contacts. These results showed the potential of nonalloyed ohmic contacts for improving high-frequency performance of the transistor.

Fig. 9 shows the evolution of f_t and $f_{\max}$ from the magnitudes in decibels versus frequency. The extrapolation by a slope of -20 dB/dec helps evaluate f_t and $f_{\max}$ for devices having alloyed and nonalloyed ohmic contacts.

The difference in high-frequency performance was attributed to lower R_{tot} and higher g_m. This result is consistent with the well-known expression for the limiting frequency of current amplification f_t. Here, R_s and R_d are the resistances of the source and drain, C_{gs} is the gate–source capacitance, and v_e is the drift velocity of electrons.

The dependence of $f_{\max}$ on f_t can be expressed as follows

$$f_{\max} \approx \frac{f_t}{2\sqrt{(R_i + R_s + R_g)g_{ds} + (2f_t)R_g C_{gd}}}. \quad (1)$$

R_i, R_s, and R_g are the channel, source, and gate resistance, respectively. C_{gd} is the gate–drain parasitic resistance, and g_{ds} is the output conductance.

For Ti-based alloyed ohmic contacts, a current gain cut of frequency (f_t) of 33.5 GHz and a maximum oscillation frequency ($f_{\max}$) of 67.5 GHz were obtained with the gate length of 0.15 μm with a device geometry of $6 \times 75\ \mu$m and the *S–D* spacing was 2.5 μm. For the MOCVD regrown InGaN nonalloyed ohmic contacts, a current gain cut of

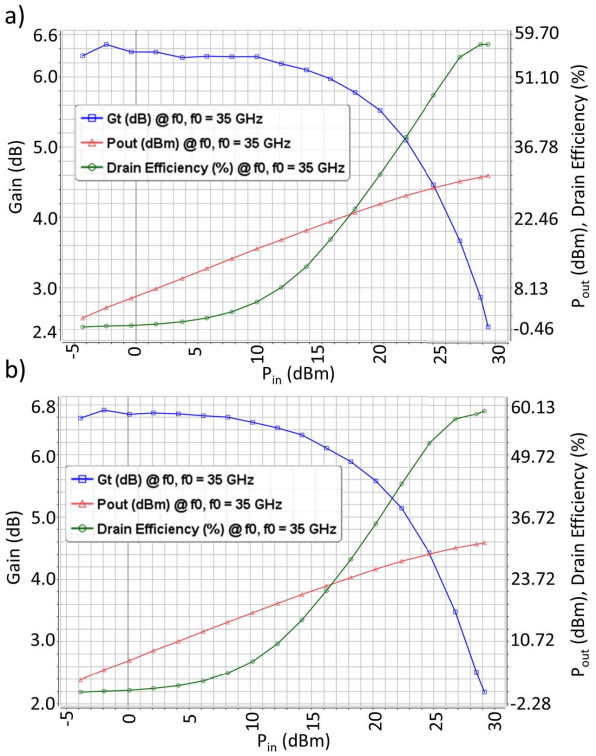

Fig. 10. Power performance of (a) alloyed and (b) nonalloyed 6×75 μm HEMT with $L_g = 0.15$ μm and S–D spacing is 2.5 μm at 35 GHz.

frequency (f_t) of 36.8 GHz and a maximum oscillation frequency ($f_{\max}$) of 75.0 GHz were obtained with the gate length of 0.15 μm with a device geometry of 6×75 μm and the S–D spacing was 2.5 μm. A notable improvement of small-signal performance, with lower R_{on} and higher g_m, was obtained for nonalloyed regrowth InGaN ohmic contacts compared with alloyed ohmic contacts.

Load-pull measurements were performed using an on-wafer measurement system from Maury Microwave to compare the power performance of the fabricated HEMTs with alloyed and nonalloyed ohmic contacts at 35 GHz for the fabricated 6×75 μm (0.45 mm) devices with an L_g of 0.15 μm.

The devices were biased at $V_{\text{ds}} = 20$ V with a quiescent current of 100 mA/mm. As shown in Fig. 10, the maximum drain efficiency of the fabricated HEMTs with alloyed ohmic contacts is almost 60% which is 3% higher compared with HEMT with alloyed ohmic contacts. At 3-dB compression, HEMT with the MOCVD regrown InGaN nonalloyed and Ti-based alloyed ohmic contacts has 31.42 and 31.02 dBm output power which corresponds to 3.07 and 2.80 W/mm, respectively. The improved power performance of the HEMTs with nonalloyed ohmic contacts can be attributed to the increase in I_{ds}, g_m, and reduced contact and ON-resistances.

IV. Conclusion

In summary, the MOCVD regrown InGaN nonalloyed ohmic contacts have been adopted on AlGaN/GaN HEMTs designed for *Ka*-band applications. The use of degenerate doped InGaN regrown nonalloyed ohmic contacts resulted in decreasing R_{tot} from 0.43 to 0.30 Ω·mm and much better surface morphology and edge acuity which are crucial for downscaled HEMTs designed for *Ka*-band applications. The MOCVD regrown InGaN nonalloyed ohmic contacts exhibited improved dc and RF performances compared with the Ti-based alloyed ohmic contacts. The 0.15-μm T-gate HEMTs fabricated with the MOCVD regrown InGaN nonalloyed ohmic contacts exhibited a maximum transconductance of 337 mS/mm, a current gain cut of frequency f_t of 36.8 GHz, and a maximum oscillation frequency $f_{\max}$ of 75 GHz. Fabricated HEMT devices on SI-SiC substrates have a maximum power density of 3.07 W/mm at 35 GHz where the device was biased at $V_{\text{ds}} = 20$ V with a quiescent current of 100 mA. High-power and high-frequency performance could be further improved by tuning the device geometry and epitaxial design.

References

[1] U. K. Mishra, P. Parikh, and Y.-F. Wu, "AlGaN/GaN HEMTs-an overview of device operation and applications," *Proc. IEEE*, vol. 90, no. 6, pp. 1022–1031, Jun. 2002.

[2] N. Ikeda *et al.*, "GaN power transistors on Si substrates for switching applications," *Proc. IEEE*, vol. 98, no. 7, pp. 1151–1161, Jul. 2010.

[3] Y. K. Lin *et al.*, "High-performance GaN MOSHEMTs fabricated with ALD Al_2O_3 dielectric and NBE gate recess technology for high frequency power applications," *IEEE Electron Device Lett.*, vol. 38, no. 6, pp. 771–774, Jun. 2017, doi: 10.1109/LED.2017.2696569.

[4] F. Roccaforte *et al.*, "Emerging trends in wide band gap semiconductors (SiC and GaN) technology for power devices," *Microelectron. Eng.*, vols. 187–188, pp. 66–77, Feb. 2018, doi: 10.1016/j.mee.2017.11.021.

[5] J. Guo *et al.*, "MBE-regrown ohmics in InAlN HEMTs with a regrowth interface resistance of 0.05 Ω·mm," *IEEE Electron Device Lett.*, vol. 33, no. 4, pp. 525–527, Apr. 2012, doi: 10.1109/LED.2012.2186116.

[6] T. Huang, X. Zhu, and K. M. Lau, "Enhancement-mode AlN/GaN MOSHFETs on Si substrate with regrown source/drain by MOCVD," *IEEE Electron Device Lett.*, vol. 33, no. 8, pp. 1123–1125, Aug. 2012, doi: 10.1109/LED.2012.2198911.

[7] H. Yu *et al.*, "Ion implanted AlGaN-GaN HEMTs with nonalloyed ohmic contacts," *IEEE Electron Device Lett.*, vol. 26, no. 5, pp. 283–285, May 2005, doi: 10.1109/LED.2005.846583.

[8] R. Wang *et al.*, "210-GHz InAlN/GaN HEMTs with dielectric-free passivation," *IEEE Electron Device Lett.*, vol. 32, no. 7, pp. 892–894, Jul. 2011, doi: 10.1109/LED.2011.2147753.

[9] F. M. Mohammed, L. Wang, D. Selvanathan, H. Hu, and I. Adesida, "Ohmic contact formation mechanism of Ta/Al/Mo/Au and Ti/Al/Mo/Au metallizations on AlGaN/GaN HEMTs," *J. Vac. Sci. Technol. B, Microelectron.*, vol. 23, no. 6, p. 2330, 2005, doi: 10.1116/1.2101691.

[10] F. Recht *et al.*, "Nonalloyed ohmic contacts in AlGaN/GaN HEMTs by ion implantation with reduced activation annealing temperature," *IEEE Electron Device Lett.*, vol. 27, no. 4, pp. 205–207, Apr. 2006, doi: 10.1109/LED.2006.870419.

[11] H.-Y. Guo *et al.*, "High-frequency AlGaN/GaN high-electron-mobility transistors with regrown ohmic contacts by metal-organic chemical vapor deposition," *Chin. Phys. Lett.*, vol. 32, no. 11, Nov. 2015, Art. no. 118501, doi: 10.1088/0256-307X/32/11/118501.

[12] B. Song *et al.*, "Ultralow-leakage AlGaN/GaN high electron mobility transistors on Si with non-alloyed regrown ohmic contacts," *IEEE Electron Device Lett.*, vol. 37, no. 1, pp. 16–19, Jan. 2016, doi: 10.1109/LED.2015.2497252.

[13] S. Ganguly *et al.*, "AlGaN/GaN HEMTs on Si by MBE with regrown contacts and FT=153 GHz," *Phys. Status Solidi*, vol. 11, nos. 3–4, pp. 887–889, Mar. 2014.

[14] J. Wu and W. Walukiewicz, "Band gaps of InN and group III nitride alloys," *Superlattices Microstruct.*, vol. 34, nos. 1–2, pp. 63–75, Jul. 2003, doi: 10.1016/j.spmi.2004.03.069.

[15] W. Walukiewicz *et al.*, "Structure and electronic properties of InN and In-rich group III-Nitride alloys," *J. Phys. D, Appl. Phys*, vol. 39, pp. 83–99, Feb. 2006, doi: 10.1088/0022-3727/39/5/R01.

[16] N. M. Shrestha, P. Chauhan, Y.-Y. Wong, Y. Li, S. Samukawa, and E. Y. Chang, "Low resistive InGaN film grown by metalorganic chemical vapor deposition," *Vacuum*, vol. 171, Jan. 2020, Art. no. 108974, doi: 10.1016/j.vacuum.2019.108974.